Int. J. Heat Mass Transfer. Vol. 29, No. 12, pp. 1989–1993, 1986
Printed in Great Britain

0017–9310/86 $3.00+0.00
Pergamon Journals Ltd.

TECHNICAL NOTES

CHF prediction via Katto's correlations and Whalley's model using AECL CHF data bank

S. C. CHENG and S. K. CHIN
Department of Mechanical Engineering, University of Ottawa, Canada

(*Received* 1 *November* 1985 *and in final form* 19 *February* 1986)

INTRODUCTION

THE ACCURATE prediction of critical heat flux (CHF) for a reactor under operating conditions and during accidental conditions is of paramount importance. In general, *ad hoc* CHF correlations are used to predict CHF. Unfortunately, this limits the application to a narrow range of flow conditions. Recently, a CHF tabular approach has been proposed [1, 2] which covers a much wider range of flow parameters. The tabular approach employs a statistical model using the Chalk River CHF data bank, which holds about 15,000 data points at the present time, as an input. Table 1 [1] lists the test conditions of AECL's CHF data bank.

In this paper, as part of current efforts in seeking the best CHF predicting method, the studies [3] based on Katto's recent correlations [4–6] and Whalley's model [7] using the CHF data bank, will be reported. Their prediction accuracy will be compared along with those of Bowring [8] and Biasi [9] reported elsewhere [1]. Katto's correlations are the newest CHF correlations and are applicable to a wide range of flow parameters and flow regimes. The choice of Whalley's model is obvious, because it represents one of very few mechanistic models available to predict CHF.

KATTO'S CORRELATIONS

Recently, Katto published a series of papers involving generalized CHF correlations, only three of them [4–6] were used directly in our present investigation. The CHF with saturated liquid at inlet q_{co}, can be expressed as

$$\frac{q_{c0}}{GH_{fg}} = \text{const.}\left(\frac{\rho_v}{\rho_l}\right)^{0.133}\left(\frac{\sigma\rho_l}{G^2 l}\right)^{1/3} \times\left\{1\Big/\left[1+\text{const.}\left(\frac{\rho_l}{\rho_v}\right)^{m}\left(\frac{\alpha\rho_l}{G^2 l}\right)^{n}\frac{l}{d}\right]\right\}. \quad (1)$$

Based on thermohydraulic consideration and world data, Katto proposed four characteristic regimes of CHF, i.e. L (low mass velocity), H (high mass velocity), N (non-linear) and HP (high pressure) regimes plus VL regime. The CHF or q_c is related to q_{c0} by

$$q_c = q_{c0}\left(1+K\frac{\Delta H_i}{H_{fg}}\right). \quad (2)$$

The linear relationship of $q_c - \Delta H_i$ only exists in L, H and HP regimes.

Using the energy balance equation, one can replace ΔH_i in equation (2) by x (exit quality) and other quantities. The revised equation (2) can then be combined with equation (1) (which has been modified slightly based on available data) to yield the following q_c equations

For L regime [4]

$$\frac{q_c}{GH_{fg}} = C\left(\frac{\alpha\rho_l}{G^2 l}\right)^{0.043}(K_L x-1)\Big/\left\{\left[K_L\left(\frac{\alpha\rho_l}{G^2 l}\right)^{0.043}-1\right]\frac{l}{d}\right\} \quad (3)$$

where C varies between 0.25 and 0.34 or can be expressed as [6]

$$C = 0.25+\frac{(l/d)-50}{150-50}(0.34-0.25) \quad (4)$$

and K_L varies between 1 and 1.16 or can be derived based on the boiling length concept as [5]

$$K_L = 1.043\Big/\left[4C\left(\frac{\sigma\rho_l}{G^2 l}\right)^{0.043}\right]. \quad (5)$$

For H regime [4, 5]

$$\frac{q_c}{GH_{fg}} = 0.10\left(\frac{\rho_v}{\rho_l}\right)^{0.133}\left(\frac{\sigma\rho_l}{G^2 l}\right)^{1/3} \times(1-K_H x)\Big/\left\{1+\left[0.0031-0.4K_H\left(\frac{\rho_v}{\rho_l}\right)^{0.133} \times\left(\frac{\sigma\rho_l}{G^2 l}\right)^{1/3}\right]\frac{l}{d}\right\} \quad (6)$$

with

$$K_H = \frac{5}{6}\left(0.124+\frac{d}{l}\right)\Big/\left[\left(\frac{\rho_v}{\rho_l}\right)^{0.133}\left(\frac{\sigma\rho_l}{G^2 l}\right)^{1/3}\right]. \quad (7)$$

For HP regime

$$\frac{q_c}{GH_{fg}} = 0.384\left(\frac{\rho_v}{\rho_l}\right)^{0.6}\left(\frac{\sigma\rho_l}{G^2 l}\right)^{0.173} \times(1-K_{HP}x)\Big/\left\{1+\left[0.28\left(\frac{\sigma\rho_l}{G^2 l}\right)^{0.233} -0.1536\left(\frac{\rho_v}{\rho_l}\right)^{0.6}\left(\frac{\sigma\rho_l}{G^2 l}\right)^{0.173}\right]\left(\frac{l}{d}\right)\right\} \quad (8)$$

with the expression of K_{HP} [6] as

$$K_{HP} = 1.12\left[1.52\left(\frac{\sigma\rho_l}{G^2 l}\right)^{0.233}+\frac{d}{l}\right]\Big/\left[\left(\frac{\rho_v}{\rho_l}\right)^{0.6}\left(\frac{\sigma\rho_l}{G^2 l}\right)^{0.173}\right]. \quad (9)$$

Notice here that the correlation for the HP regime was

NOMENCLATURE

C	constant in equations (3) and (4) or concentration
C_{EQ}	equilibrium concentration
D	deposition mass flux
d	diameter
E	entrainment mass flux
G	mass flux
H_{fg}	latent heat
K	constant, depending on flow regimes
k	mass transfer coefficient
l	length
p	pressure
q_c	critical heat flux
q_{co}	q_c with $\Delta H_i = 0$
x	exit quality
z	coordinate.

Greek symbols

α	void fraction
ΔH	subcooled enthalpy
ρ	density
σ	surface tension.

Subscripts

H	H (high mass velocity) regime
HP	HP (high pressure) regime
i	inlet
L	L (low mass velocity) regime
LF	liquid film
l	liquid
v	vapor.

Table 1. Critical heat flux data bank: range of data [1]

Ref.*	Presure (MPa)	Mass flux (10^3 kg m^{-2} s^{-1})	Dryout quality	ΔH_i (MJ kg^{-1})	Length (m)	Diam. (cm)	CHF (MW m^{-2})	No. of points
Anon [4]	7.9–20.0	0.3–2.8	−0.10–0.74	0.60–1.40	1.00–2.00	1.00	1.10–5.5	118
Mayinger [5]	1.9–10.2	2.2–3.7	0.10–0.41	−0.20–0.30	0.80–1.40	0.700	0.90–5.6	128
Era [6]	6.9–7.1	1.1–3.0	0.37–0.95	−1.20–0.60	1.60–4.8	0.598	0.10–2.0	163
Tong [7]	5.2–13.8	0.7–13.4	0–0.50	0–14.0	0.40–3.7	0.6–1.3	0.60–6.1	265
Thompson [3]								
Table 1	0.103	0.01–5.70	0–1.0	0–0.4	0.03–0.86	0.1–2.4	0.20–19.3	106
2	0.690	0.01–0.09	0.74–1.0	−0.1–0.5	0.24	0.457	0.10–1.0	20
3	1.7–2.1	0.06–15.7	−0.03–0.78	0–0.7	0.11–0.15	0.11–0.31	0.20–21.4	55
4	3.4–4.4	0.04–10.6	−0.02–1.03	0.01–0.9	0.08–1.7	0.31–1.08	0.30–9.0	272
5	4.7–5.2	1.00–8.1	0.01–0.90	0–0.4	0.30–1.7	0.46–0.56	1.50–6.8	37
6	6.8–7.3	0.03–10.4	−0.21–1.58	0.01–1.1	0.08–3.7	0.37–3.8	0.40–9.4	827
7	8.8–9.1	1.00–4.1	0.07–0.52	0.07–0.4	0.60–1.5	0.57–1.1	1.60–2.4	19
8	10.3–11.1	0.03–9.9	−0.20–1.2	0.08–1.3	0.23–1.5	0.46–2.0	0.30–10.8	234
9	12.1–12.4	0.40–4.1	−0.07–0.40	0.10–1.4	0.15–0.91	0.19–2.0	1.40–5.4	62
10	13.790	0.04–10.6	−0.46–0.98	0–1.5	0.08–1.8	0.19–1.1	0.30–14.8	638
11	15.514	2.00–3.9	−0.11–0.01	0.40–1.5	0.15–0.70	0.191	2.00–6.6	30
12	17.238	1.90–3.7	−0.14–0.05	0.40–0.8	0.15–0.70	0.191	2.80–5.1	30
13	18.272	0.80–2.90	−0.12–0.01	0.05–0.4	0.04–0.15	0.300	1.10–2.4	10
14	18.961	1.80–3.8	−0.38–0.08	0.50–1.7	0.15–0.70	0.191	2.10–5.2	30
15	0.2–4.1	0.10–2.4	0.20–1.05	0.08–0.9	0.60–3.10	0.39–1.0	0.30–5.1	1572
Becker [8]								
Table 1.1	0.2–5.8	0.20–1.9	0.42–0.99	−0.05–0.8	1.00–3.10	0.39–0.99	0.30–1.8	571
1.2	0.2–3.7	0.10–2.5	−0.07–0.94	0.20–1.6	0.40–3.00	0.99–1.30	0.50–7.5	1786
1.3	1.0–4.1	0.20–3.2	0.09–0.90	0.20–0.9	1.00–3.20	0.61–2.00	0.70–5.1	273
1.4	1.1–8.9	0.20–5.0	−0.01–0.95	0.20–2.7	1.00–3.80	0.39–2.50	0.50–5.4	843
Becker [9]	8–20	0.156–7.56	−0.3–0.98	—	1.00–4.97	1.00	0.13–5.5	1598
Cheng [10]	0.10–0.69	0.05–0.20	0.19–1.22	0.04–0.21	0.37–0.74	1.23	0.33–2.1	150
Menegus [11]	0.19–6.8	0.006–13.7	−0.21–0.0	0.0–0.6	0.0	0.36–9.24	1.56–11.7	129
Bergles [12]	0.206	3.04–6.08	−0.037	81.0	0.0	0.46–0.61	4.9–6.0	3
Lowdermilk [13]	0.1	0.03–4.87	0.03–1.0	0.32–0.33	0.12–0.96	0.40–0.48	0.17–9.5	113
Zenkevich [14]								
Table 16	58.9	0.5–5.1	0–0.95	0.07–1.0	1.00–6.00	0.6–1.1	0.35–5.8	273
18	68.7	0.5–5.1	0–0.96	0–1.1	1.00–6.00	0.6–1.3	0.32–6.5	517
20	78.5	0.5–5.1	−0.02–0.97	0.07–0.99	1.00–6.00	0.6–1.1	0.33–6.3	292
22	98.1	0.5–5.9	−0.06–0.93	0–12.4	1.00–6.00	0.5–1.1	0.24–7.2	594
24	117.9	0.5–6.0	−0.13–0.79	0.02–13.3	1.00–6.00	0.5–1.1	0.18–7.0	610
26	137.3	0.5–5.1	−0.22–0.61	0–13.9	1.00–6.00	0.5–1.1	0.16–7.3	777
28	147.1	0.5–6.1	−0.29–0.70	0–13.1	1.00–6.00	0.1–8.2	0.14–7.1	476
30	157.0	0.5–5.1	−0.41–0.71	0.04–14.9	1.00–6.00	0.6–1.1	0.14–7.1	509
32	176.6	0.5–6.7	−0.80–0.61	0.05–15.4	1.00–6.00	0.5–1.1	0.14–5.7	753
34	196.2	0.5–5.1	−0.98–0.80	0.05–16.3	1.00–6.00	0.6–1.1	0.14–4.9	559

* Numbers in square brackets are reference numbers from Groeneveld *et al.* [1].

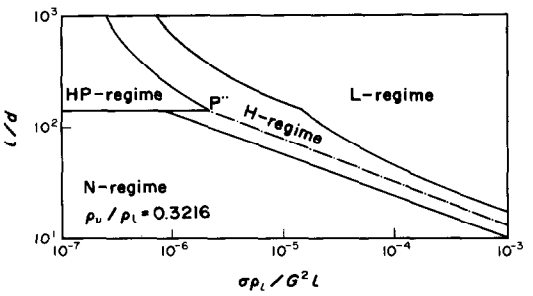

FIG. 1. Boundaries for L, H, N and HP regimes [6].

derived by us based on new q_{c0} and the boiling length concept [6].

As mentioned previously, there is no correlation in the N regime. However, data points which are within N regime but near H regime (small ΔH_i) may be evaluated approximately as the following (which was derived by us)

$$\frac{q_c}{GH_{fg}} = 0.098\left(\frac{\rho_v}{\rho_l}\right)^{1.333}\left(\frac{\sigma\rho_l}{G^2 l}\right)^{0.443}\frac{(l/d)^{0.27}}{1+0.0031(l/d)} \times (1-Kx)\Big/\left[1-0.392K\left(\frac{\rho_v}{\rho_l}\right)^{1.333} \times\left(\frac{\sigma\rho_l}{G^2 l}\right)^{0.443}\frac{(l/d)^{1.27}}{1+0.0031(l/d)}\right] \quad (10)$$

with the expression of K [5] as

$$K = \left[0.416\left(0.0221+\frac{d}{l}\right)\left(\frac{d}{l}\right)^{0.27}\right]\Big/\left[\left(\frac{\rho_v}{\rho_l}\right)^{0.133}\left(\frac{\sigma\rho_l}{G^2 l}\right)^{0.433}\right]. \quad (11)$$

Boundary equations between various regimes can be found in ref. [6] and a typical map for various regimes is shown in Fig. 1 [6].

To test the accuracy of any correlation, the CHF for each data point of the CHF data bank was predicted in two ways:

(1) Constant dryout quality: CHF $= f(p, G, x, d)$.
(2) Constant inlet subcooling: CHF $= f(p, G, l, d, \Delta H_i)$. This method requires an intermediate step: the calculation of the dryout quality from the heat balance.

Table 2 summarizes the comparison of prediction accuracy for different regimes in Katto's correlations based on constant dryout quality. Two cases of C and K_L constants are presented. The first case with $C = 0.34$ and $K_L = 1.0$ gives the best overall prediction within the ranges of constants suggested by Katto. In the second case with K set to 0.5 (which is outside the range given by Katto), it improves slightly the results over the first case. Prediction accuracy based on constant inlet subcooling is presented in Table 3. In general, they predict much more accurate CHF values than the constant dryout quality case. However, their prediction is not very sensitive to the values of C and K_L. In all cases, Katto's correlations in the HP regime always yield the best results.

WHALLEY'S MODEL

Whalley *et al.* [7] developed a CHF model for annular flow, based on the assumption that CHF occurs when the liquid film flow on the channel wall is reduced to zero. They arbitrarily assumed the annular flow to start at 1% quality and predicted the change in liquid film flow using the mass balance from

$$\frac{dG_{LF}}{dz} = \frac{4}{d}\left(D - E - \frac{q_{c0}}{\lambda}\right) \quad (12)$$

where $D = kC$ and $E = kC_{EQ}$.

Empirical values of k were given as a function of surface tension. C was provided theoretically while C_{EQ} was given empirically. Only the case involving prediction of CHF by iterating the predicted tube length to match the experimental tube length will be presented here. Other cases such as predicting the burnout boiling length or dryout quality from a given heat flux were presented in ref. [3].

COMPARISON OF PREDICTING METHODS

Prediction results from Katto's, Bowring's and Biasi's correlations are shown in Table 4 based on constant dryout quality. Biasi and Katto give a better prediction than Bowring. Table 5 compares prediction from various methods based on constant inlet subcooling. The results from Whalley's model are also included for comparison. Strictly speaking, Whalley's model is not based on constant inlet subcooling, instead, it iterates the predicted tube length to match the experimental tube length. Bowring and Biasi yield better prediction accuracy than Katto.

Table 2. Comparison of prediction accuracy for different regimes in Katto's correlations based on constant dryout quality

Regime	Error bounds ±10%	±20%	±50%	Number of valid data	Average error*	r.m.s. error
$C = 0.34$; $K_L = 1.0$						
L	5.38	11.61	35.83	2679	−0.4741	0.6705
H	20.44	43.58	81.87	5411	0.1103	0.5736
N	0.0	0.0	0.0	0	0.0	0.0
HP	39.66	72.51	99.27	411	0.0732	0.1850
NH	21.35	55.08	95.33	857	−0.1240	0.2748
All regimes	17.05	36.75	70.69	9358	−0.0800	0.5721
$C = 0.34$; $K_L = 0.5$						
L	10.63	26.12	94.63	2680	−0.2458	0.3423
H	20.44	43.58	81.87	5411	0.1103	0.5736
N	0.0	0.0	0.0	0	0.0	0.0
HP	39.66	72.51	99.27	411	0.0732	0.1850
NH	21.35	55.08	95.33	857	−0.1240	0.2748
All regimes	18.56	40.90	87.52	9359	−0.0147	0.4818

* Average error refers to arithmetic error.

Table 3. Comparison of prediction accuracy for different regimes in Katto's correlations based on constant inlet subcooling

Regime	Error bounds ±10%	±20%	±50%	Number of valid data	Average error	r.m.s. error
$C = 0.34$; $K_L = 1.0$						
L	24.23	73.87	99.66	2679	−0.1275	0.1726
H	64.28	92.22	98.95	5411	0.0064	0.1476
N	0.0	0.0	0.0	0	0.0	0.0
HP	91.73	100.00	100.00	411	0.0233	0.0569
NH	49.01	83.31	99.30	857	−0.0799	0.1622
All regimes	52.62	86.49	99.23	9358	−0.0391	0.1539
$C = 0.34$; $K_L = 0.5$						
L	20.52	58.88	99.37	2680	−0.1467	0.2030
H	64.28	92.22	98.95	5411	0.0064	0.1476
N	0.0	0.0	0.0	0	0.0	0.0
HP	91.73	100.00	100.00	411	0.0233	0.0569
NH	49.01	83.31	99.30	857	−0.0799	0.1622
All regimes	51.55	82.20	99.15	9359	−0.0446	0.1642

Table 4. Comparison of prediction accuracy for different prediction methods based on constant dryout quality

Prediction method	Error bounds ±10%	±20%	±50%	Number of valid data	Average error	r.m.s. error
Katto						
$C = 0.34$; $K_L = 1.0$	17.05	36.75	70.69	9358	−0.0800	0.5721
$C = 0.34$; $K_L = 0.5$	18.56	40.90	85.72	9359	−0.0147	0.4818
Bowring	30.79	53.13	79.26	10214	0.1619	0.7555
Biasi	21.32	41.13	73.04	9935	−0.0925	0.4359

Table 5. Comparison of prediction accuracy for different prediction methods based on constant inlet subcooling

Prediction method	Error bounds ±10%	±20%	±50%	Number of valid data	Average error	r.m.s. error
Katto						
$C = 0.34$; $K_L = 1.0$	52.62	86.49	99.23	9358	−0.0391	0.1539
$C = 0.34$; $K_L = 0.5$	51.55	82.20	99.15	9359	−0.0446	0.1642
Bowring	85.62	97.10	99.57	10124	0.0148	0.0928
Biasi	77.60	96.60	99.91	9935	−0.0209	0.0936
Whalley*	16.95	36.44	73.31	3499	−0.1922	0.4306

* Whalley's model is not based on constant inlet subcooling, instead, it iterates the predicted tube length to match the experimental tube length.

CONCLUSIONS

1. Katto's correlations give a better prediction than Whalley's model in terms of accuracy, range of flow parameters and computation time.
2. Based on constant dryout quality, Biasi's and Katto's correlations predict better results than that of Bowring.
3. Based on constant inlet subcooling, Bowring's and Biasi's correlations yield better prediction than that of Katto.
4. In all cases, Katto's correlation in the HP regime gives the best results.

REFERENCES

1. D. Groeneveld, S. C. Cheng and T. Doan, The CHF look-up table, a simple and accurate method for predicting critical heat flux, submitted to *Heat Transfer Engng.*
2. S. C. Cheng, K. T. Heng and T. Doan, Construction of CHF table, *Proc. 1984 Summer Computer Simulation Conference*, Boston, Vol. 2, pp. 702–704 (1984).
3. S. K. Chin, The comparison of prediction methods for flowing boiling CHF. M. Eng. report, University of Ottawa (1985).
4. Y. Katto, A generalized correlation of critical heat flux for the forced convection boiling in vertical uniformly heated round tubes, *Int. J. Heat Mass Transfer* **21,** 1527–1542 (1978).
5. Y. Katto, An analysis of the effect of inlet subcooling on critical heat flux of forced convection boiling in vertical uniformly heated tubes, *Int. J. Heat Mass Transfer* **22,** 1567–1575 (1979).
6. Y. Katto, Critical heat flux of forced convection boiling in uniformly heated vertical tubes (correlation of CHF in HP regime and determination of CHF regime map), *Int. J. Heat Mass Transfer* **23,** 1573–1580 (1980).

7. P. B. Whalley, P. Hutchinson and P. W. James, The calculation of critical heat flux in complex situation using an annular flow model, *Proc. 6th Int. Heat Transfer Conference*, Toronto, Vol. 5, pp. 65–70 (1978).
8. R. W. Bowring, A simple but accurate round tube, uniform heat flux dryout correlation over the pressure range 0.7–17.0 MN/m^2, AEEW-R789 (1972).
9. L. Biasi, G. C. Clerici, S. Garribba, R. Sala and A. Tozzi, Studies on burnout: Part 3, *Energia nucl., Milano* **14**, 530–536 (1967).

Int. J. Heat Mass Transfer. Vol. 29, No. 12, pp. 1993–1996, 1986
Printed in Great Britain

0017–9310/86 $3.00 + 0.00
Pergamon Journals Ltd.

Second-order boundary layers for steady, incompressible, three-dimensional stagnation point flows

R. VASANTHA and G. NATH*
Department of Applied Mathematics, Indian Institute of Science, Bangalore-560012, India

(*Received* 12 *December* 1984 *and in final form* 20 *January* 1986)

INTRODUCTION

IT IS well known that the classical boundary-layer theory represents the asymptotic solution of the Navier–Stokes equations for large Reynolds numbers. The succeeding approximation is the second-order boundary layer one which includes the effects of surface curvature, vorticity interaction and boundary-layer displacement. The second-order boundary-layer effects become important when the boundary-layer thickness becomes comparable with the characteristic body length. Van Dyke [1] and Gersten and Gross [2] have given an excellent survey of higher-order boundary layers.

The second-order boundary-layer effects on the steady, laminar, incompressible, three-dimensional stagnation point flow with or without mass transfer was considered by Papenfuss [3, 4] for nodal point flows where only the curvature and displacement effects were taken into account. Subsequently, Gersten *et al.* [5] extended the foregoing analysis to include the effect of Prandtl number without mass transfer in nodal point region taking into account only curvature effect. It may be remarked that all the second-order boundary-layer effects in the saddle point region and vorticity interaction effect in the nodal point region have not been considered so far.

The aim of this study is to consider the combined effect of Prandtl number and mass transfer on the second-order boundary layers in both nodal and saddle point regions of a three-dimensional body in the neighbourhood of the stagnation point. The governing equations have been solved using an implicit finite-difference scheme. The results have been compared with those available in the literature.

GOVERNING EQUATIONS

The steady, laminar, incompressible boundary-layer flow with mass transfer in the stagnation region of a three-dimensional body having two planes of symmetry is considered (Fig. 1). The first- and second-order boundary-layer equations governing the flow in the neighbourhood of a stagnation point of a three-dimensional body can be derived from the Navier–Stokes equations using the matched asymptotic expansion. Since the detailed derivation is presented in refs. [3, 4], here we write the equations in dimensionless form as:

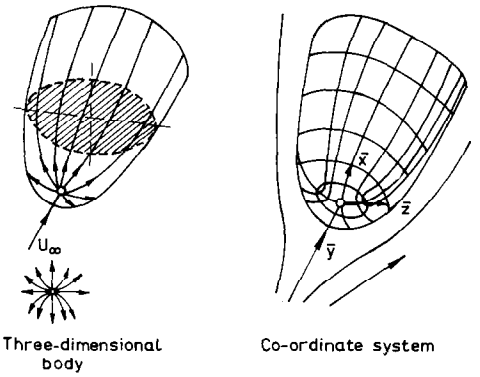

FIG. 1. Coordinate system.

First-order equations

$$f'''+(f+cg)f''+1-f'^2=0 \tag{1a}$$

$$g'''+(f+cg)g''+c-cg'^2=0 \tag{1b}$$

$$\theta''+Pr(f+cg)\theta'=0. \tag{1c}$$

The boundary conditions are

$$f(0)=f_w,\quad f'(0)=0,\quad g(0)=0,\quad g'(0)=0,$$
$$\theta(0)=0,\quad f'(\infty)=1,\quad g'(\infty)=1,\quad \theta(\infty)=1 \tag{2}$$

where

$$\eta=U_{11}^{1/2}k_{x0}Re^{1/2}y,\quad \varepsilon=Re^{-1/2},\quad Re=U_\infty\rho/k_{x0}\mu,$$
$$c=W_{11}/U_{11}=[(dW_1/dz)/(dU_1/dx)]_0. \tag{3}$$

Second-order equations

1. Longitudinal curvature

$$D_1(F_L,G_L)=A_1f''+\eta(1-f'^2)+A_3-c\chi+\eta(1-c)+cA_2 \tag{4a}$$

$$D_2(F_L,G_L)=g'(f+cg)+g''+A_1g''-c\eta(1+g'^2) \tag{4b}$$

$$D_3(H_L)=-\theta'-Pr\,\theta'[F_L+cG_L-A_1]. \tag{4c}$$

Boundary conditions:

$$\eta=0:\ F_L=F_L'=G_L=G_L'=H_L=0 \tag{5a}$$

$$\eta\to\infty:\ F_L'\to-\eta,G_L'\to\eta,H_L\to0. \tag{5b}$$

2. Transverse curvature

$$D_1(F_t,G_t)=A_1f''-\eta(1+f'^2)+f'(f+cg)+f'' \tag{6a}$$

$$D_2(F_t,G_t)=A_1g''+\eta c(1-g'^2)+A_3-\chi+\eta(c-1)+A_2 \tag{6b}$$

$$D_3(H_t)=-\theta'-Pr\,\theta'[F_t+cG_t-A_1]. \tag{6c}$$